

DNA-Liposome Hybrid Carriers for Triggered Cargo Release

*Kevin N. Baumann^{1,2†}, Tim Schröder³, Prashanth S. Ciryam^{1‡}, Diana Morzy^{2§}, Philip Tinnefeld^{3,4},
Tuomas P. J. Knowles^{1,2*}, Silvia Hernández-Ainsa^{5,6*}*

AUTHOR ADDRESSES

1 Yusuf Hamied Department of Chemistry, University of Cambridge, Lensfield Road, Cambridge CB2 1EW, United Kingdom

2 Cavendish Laboratory, University of Cambridge, JJ Thomson Avenue, Cambridge CB3 0HE, United Kingdom

3 Department of Chemistry, Ludwig Maximilian University München, Butenandtstr. 5 – 13, 81377 Munich, Germany

4 Center for NanoScience, Ludwig Maximilian University München, Geschwister-Scholl Platz 1, 80539 Munich, Germany

5 Instituto de Nanociencia y Materiales de Aragón, CSIC–Universidad de Zaragoza, Zaragoza 50009, Spain

6 ARAID Foundation, Government of Aragon, Zaragoza 50018, Spain

KEYWORDS DNA nanotechnology; biomimetics; liposome; triggered release; drug delivery

ABSTRACT The encapsulation of chemotherapeutics by biocompatible carrier structures holds great promise to preserve their therapeutic activity and favor their delivery to tumor sites. To enhance the bioavailability of a drug at the targeted tissue, triggered release mechanisms have received increasing research interest. Many approaches rely on exogenous triggers such as the irradiation of ultrasound, visible or even ionizing electromagnetic waves. However, such exogenous triggers can be challenging to implement in a specific manner. Therefore, designing carriers responsive to endogenous moieties, such as nucleic acid biomarkers, is a desirable step in the search of personalized drug delivery nanoplatforms. This study presents an approach to building a biocompatible DNA-liposome hybrid nanocarrier for potential triggered release purposes. We form a DNA mesh on large unilamellar liposomes incorporating a trigger-responsive DNA building block. Upon incubation with a single-stranded DNA trigger sequence a hairpin closes and the building block is allowed to self-contract. By this process, we demonstrate elevated release of the dye calcein and the drug doxorubicin. The incubation of the doxorubicin-laden active hybrid carrier with HEK293T cells suggests increased cytotoxicity relative to a control carrier without the triggered release mechanism. In the future, the trigger could be provided by peritumoral nucleic acid sequences and lead to site-selective release of encapsulated chemotherapeutics.

TEXT

Treatment with many drugs, especially chemotherapeutics, can be associated with severe side effects. Following administration, drug molecules can circulate throughout the blood stream and can be internalized by a range of cells depending on their rate of metabolism – regardless of whether they are of cancerous or of healthy origin.^{1,2} Another limitation is that small molecules are generally cleared out of the organism rapidly. To address these challenges, the development of larger carrier constructs has shown promise, especially if these are targeted.^{3–6} Thus, the encapsulation of small therapeutic molecules by carrier structures holds great potential to maximize delivery efficiency. To fulfil a therapeutic effect, however, the drug must become bioavailable by being released from the carrier.^{7–9} This requires the precise control over the mechanism and timing of cargo release.⁷

Exogenous triggers, such as electromagnetic radiation, allow the precise timing of trigger deployment, but in many cases require additional intrusion and interference with the organism, or the use of highly specialized materials. Moreover, the irradiation of e.g. ultraviolet or visible light as trigger types is hampered by the shallow penetration depths in biological tissues.^{10–12} X-rays in particular offer greater penetration and can be used in combination with radiotherapy.^{2,13} In other applications, however, ionizing radiation imposes an additional risk. For these reasons, an entirely autonomous device with release properties dependent on an endogenous trigger event may be a preferable solution.¹⁴

DNA as a building material has great potential to create a drug delivery vehicle responding to endogenous triggers.^{15–18} The triggered hybridization of DNA can produce forces large enough to facilitate the transition between secondary structures.^{19–21} It has been previously shown that the

binding of an aptamer sequence to its target structure can displace pre-hybridized complementary DNA from the aptamer.¹⁶ This approach has the advantage that an overexpressed protein can facilitate targeted delivery and selective drug release at the same time. Interestingly, also nucleic acids can be overexpressed by tumor cells and be present at elevated concentrations in the peritumoral environment.^{22–24} The hybridization of these nucleic acids with a corresponding carrier-associated DNA motif could therefore initiate the conversion between secondary structures and thus trigger drug release by direct mechanical interference with the delivery vehicle, such as a lipid vesicle.

Lipid vesicles represent a biocompatible carrier structure that can be produced with high throughput.^{25,26} DNA can be easily anchored to the lipid bilayer mediated by chemically attached hydrophobic moieties.^{27–31} Several studies demonstrate a strong link between the conformation of the DNA structures and the shape or integrity of the lipid bilayer.^{27,32,33} However, many current approaches rely on stochastic modes of deforming lipid vesicles. Triggering the structural activation of liposome-associated DNA building blocks to affect the permeability of the lipid bilayer to specific molecules could offer a potent strategy of generating a drug delivery vehicle with a selective release feature.

This study presents a method to release small molecules from liposomes by the triggered contraction of ‘active DNA building blocks’ (aDBB). These are arranged on the surface of the liposomes and integrated into a DNA coat, following a modified assembly method of an approach which we described previously.³⁴ The addressability of the aDBB leverages the triggered self-hybridization of a DNA hairpin (H), resulting in a contraction of the aDBB. To instate control over the hairpin closure, a spacer strand (S) was pre-annealed with the hairpin to keep it in an open, or stand-by state (Figure 1a). When adding a trigger sequence (C), S can be displaced in a toehold-

mediated reaction. The HS DNA duplex (aDBB) was inserted between a cholesterol-triethylene glycol (TEG)-modified linker (L composed of L_1 and L_2 , Figure 1a) and a DNA triskelion (T) by hybridization via the oligonucleotides L_2 (part of the linker and partially complementary to H) and M (linking H to T). The cholesterol-TEG modification of L allowed the aDBB to insert into lipid membranes (Figure 1b). In this manner, several of these motifs could be connected on the surface of liposomes in a two-step polymerization process: first, the combination of the aDBB, the cholesterol-TEG-labelled L, and M (referred to as L_{HS}) was incubated with large unilamellar vesicles (LUVs). Second, the DNA triskelion was added to finalize the coating process (Figure 1c). The element-wise contraction of the DNA building blocks integrated in the DNA coat could alter the permeability of the assembled structures and facilitate the release of encapsulated molecules.

To probe the ability of the active building block to contract upon stimulation with the trigger sequence C (Figure 1a), S was modified with a Cy3 fluorophore (pink sphere, Figure 2a), whereas C was modified with a BlackHole II quencher (black sphere) in the complementary position (Figure 2a). Figure 2 shows the fluorescence signal decrease as a result of the hybridization of C and S, indicating the success of the displacement reaction. As a reference, a control sequence C_C was added (blue data trace). Here, only an insignificant drop of the fluorescence intensity due to stochastic quenching could be observed, comparable to the effect of dilution as simulated by adding pure PBS (grey data trace). Single-molecule FRET measurements were performed to measure the inter-dye distance, quantified by the FRET efficiency, upon contraction of the aDBB. To this end, the DNA strands adjacent to H were labelled with a Cy3 fluorophore (pink sphere) as donor molecule (strand L_2 , Figure 2c), and a Cy5 fluorophore (red sphere) as acceptor molecule (strand M, Figure 2c). Before addition of C, the FRET efficiency was zero (Figure 2c) which is

reasonable for an estimated donor acceptor distance of approximately 15 nm (see Supporting Information for details) and a Förster-radius of ca. 5.3 nm.³⁵ After the displacement of S, however, the FRET efficiency shifted to around 45%, which accounts for a distance of approximately 6 nm for this donor-acceptor pair (using Gamma-corrected values, see also experimental section).^{35–37} This finding suggests that the displacement of S upon hybridization with C indeed causes a contraction of up to ca. 9 nm of the building block by allowing H to self-hybridize.

To confirm the desired integration of the aDBB in the formerly established DNA coat, dynamic light scattering and ζ -potential measurements were performed. An increase of the hydrodynamic diameter was observed, accompanied by a decrease of the ζ -potential, when the DNA coats are assembled on the vesicle surfaces (Supporting Information, Figure S2). Furthermore, the addition of a detergent led to a double peak in the DLS spectrum denoting detergent-lipid micelles and coexisting DNA assemblies, as we previously described.³⁴ Next, we sought to gain further insight of the functionality of the aDBB when integrated in the DNA coats on liposomes. To this end, we studied DNA-coated giant unilamellar vesicles (GUVs) by confocal microscopy and fluorescence recovery after photobleaching (FRAP) measurements. Initially, the fluorescence recovery profiles of the ATTO550-labelled S and the ATTO647N-labelled T were measured before adding the trigger sequence C. The two species showed similar recovery kinetics and levels of recovered fluorescence (Figure 3a and c). In comparison to our previously established DNA coats without the aDBB, here a construct with higher mobility and fewer constraints is present. This may be related to lower polymerization efficiency or to the introduction of more degrees of freedom by structures of larger flexibility (additional sites of ssDNA as knickpoints, refer to Figure 1a).³⁴ After adding C, the recovery traces of S and T diverged (Figure 3b) and two populations of recovery behaviors emerge: while S shows faster recovery kinetics and higher recovered fluorescence

intensity levels (Figure 3c and d), the recovery of T is represented by slower kinetics and only marginal recovered fluorescence intensity (Figure 3e and f). This result corroborates the hypothesis that S is removed by C, which can consequently dissociate from the DNA coat and hence is not restraint in its mobility by the DNA coat anymore. These results suggest that the transition of the SC duplex into the solution is limited by steric hindrance imposed by the DNA coat, and magnesium-assisted unspecific adsorption to the lipid bilayer, which allowed the observation by FRAP with overall reduced signal intensity (relative to the ATTO647N-labelled T by approximately 50%, see also Supporting Information, Figure S3).³⁸ At the same time, the hairpin can self-hybridize and may stiffen or compact the DNA coat, as indicated by the slow recovery kinetics of T and the reduced post-bleaching fluorescence intensities which exhibit similar properties to the DNA coats we previously described.³⁴ During this process, we could not detect visible deformation or disruption of the GUVs (Supporting Information, Figure S3). By contrast, when the displacement reaction is performed under hyperosmotic pressure, membrane budding or tubulation can be observed in some cases (Figure 3g).

As an indicator of the applicability of the DNA-liposome hybrid structures as triggered-release delivery vehicles, we investigated potential changes of the permeability to entrapped small molecules. Therefore, the lipid films were rehydrated in a calcein-containing solution to generate calcein-laden LUVs. The leakage of calcein from the LUVs is expressed by an increase of the fluorescence intensity, as the consequent dilution of the fluorophore results in a loss of self-quenching which only occurs at high concentrations. Initially, we measured the passive leakage of calcein from pure liposomes (V) in comparison to the coated structures VL_{HS}T and VLT. The addition of the DNA coats, significantly reduced the leakage of calcein over the course of the measurement. To study the active release, the trigger sequence C was added to the samples V,

VL_{HS}T and VLT (as inactive control of the hybrid carriers). In contrast to VLT, the trigger-responsive carrier (VL_{HS}T) responded to the supplementation of C by an elevated permeability to the entrapped calcein, close to pure POPC liposomes (Figure 4a). In addition, we performed a control experiment where an inactive sequence C_C was incubated with VL_{HS}T. C_C did not cause a similar permeability benefit, excluding the possibility that the release was only an effect of osmotic changes.

To further explore controlled drug delivery and release applications, we produced LUVs that encapsulated the widely-used chemotherapeutic doxorubicin (DOX).^{39–41} As a model culture, HEK293T cells were then incubated with DOX-laden VL_{HS}T, and VLT. The trigger strand C was added to the DOX-laden carriers, whereby only the VL_{HS}T design is expected to respond to the trigger and increase the permeability to DOX. After the incubation time, the cytotoxic effect of the two carriers was estimated using a luciferase viability assay. Figure 4b shows that upon addition of C the toxicity of the trigger-responsive carrier design (VL_{HS}T) is significantly increased with respect to the non-responsive VLT design which we assigned to the enhanced permeability of the vesicle promoted by the activation of the aDBB.

In conclusion, in this study we demonstrate an approach to add release functionality to DNA-coated vesicles. We provide evidence that the triggered closure of a DNA hairpin can influence the DNA coat and lipid membrane properties. This effect is likely to originate from the contraction of the hairpin following its self-hybridization. This strategy can be applied to triggered release purposes, which we evidence by the release of dye molecules and the enhanced cytotoxicity induced by the DOX-laden trigger-responsive coated liposomes. In the future, the presented method may inspire similar approaches with maximized control of the deformation of liposomes. We believe that a system like this can have significant potential for nanotherapeutic applications

as it allows molecules to be transported and released only when a trigger is present. This could be exploited for instance in the proximity of tumors, where the bioavailability of enclosed molecules can be increased by triggering the release through the interaction with pathophysiologically over-expressed biomolecules and the carriers.^{3,42–46}

Method Section

Folding of the Active DNA Building Block

The aDBB was folded in two steps. First the strands S and H were hybridized using a custom thermal protocol: in 1x PBS (pH = 7.4, or an aqueous solution 75 mM Na₂HPO₄, pH = 7.4 for the leakage measurements) 6 μ M of the two oligonucleotides was suspended and heated to 85 °C for 5 min, before cooling to room temperature at a rate of -0.5 °C per minute. Eventually, the samples were kept at 4 °C. In the second step, the S-H-duplex was incubated with L (separately annealed following our previously published protocol³⁴) and the strand M. All oligonucleotides were purchased from Integrated DNA Technologies (IDT). The sequences of all involved oligonucleotide sequences can be reviewed in the Supporting Information, Table S1.

Gel Electrophoresis

Polyacrylamide gel-electrophoresis (PAGE) was performed to evaluate the folding success the DNA structures. The gels were prepared with 10% polyacrylamide in 11 mM MgCl₂ buffered at pH = 8.3 with 0.5x TBE and run for 60 min at 100 V, immersed in a solution containing 11 mM MgCl₂ buffered at pH = 8.3 with 0.5x TBE.

Fluorescence quenching measurements

The efficacy of the toehold-mediated displacement reaction in removing the spacer strand was further verified by measuring fluorescence quenching when hybridizing with the displacement strand. To this end, C was labelled with an Iowa Black-quencher in the 5'-terminal and S with a Cy3 fluorophore in the 3'-terminal (purchased from IDT). The degree of fluorescence quenching upon addition of the displacement strand correlates with the amount of displaced spacer. The aDBB was studied at a concentration of 2 μM ; the displacement strand was added at 2x excess (to increase the displacement success, following PAGE results). As a control, a non-hybridizing sequence C_C was labelled with an Iowa Black-quencher and added under the same concentration conditions. As a further control, PBS was added at the same volume as C_C to compare the stochastic quenching originating from the addition of C_C to the fluorescence reduction originating from dilution.

Single-Molecule FRET Measurements

All oligonucleotides were purchased at a concentration of 100 μM from IDT in nuclease- and salt-free buffer for the single-molecule FRET measurements. For assembling of the aDBB, the oligonucleotides were mixed according to Table S2 in aliquots of 20 μL in a solution containing 12.5 mM MgCl_2 buffered with 10x TAE. The sample solution was subjected to the thermal protocol summarized above. Finally, the mixture was purified with a 4% 1x TBE agarose gel, which was run for 30 min at 160V in the same buffer. The slowest band (formed by the desired product) was cut out and the structure was extracted by squeezing the cut-out between cover slides. Prior to the single-molecule FRET measurements, the samples were diluted in 1x PBS to achieve a concentration of 100 pM. The displacement reaction was performed by adding D at a

concentration of 8 μM . The single-molecule FRET experiments by pulsed interleaved excitation (PIE)⁴⁷ were carried out with a custom-built confocal microscope. To this end, the DNA was placed in custom-built 60 μL imaging chambers. The fluorescent donor molecules were excited by a pulsed diode laser (LDH-P- FA-530B, PicoQuant, Germany), at 532 nm operated with a 20 MHz repetition rate. The excitation intensity was adjusted to 30 μW . The fluorescent acceptor molecules were excited by a pulsed diode laser (LDH-D-C-640, PicoQuant), at 639 nm operated with a 20 MHz repetition rate. The excitation intensity of the sample was adjusted to 30 μW . The laser pulses were separated by 35 ns by a multichannel picosecond diode laser driver (PDL 828 “Sepia II”, PicoQuant) with an oscillator module (SOM 828, PicoQuant). The lasers were coupled into a single mode fiber (P3-488PM-FC, Thorlabs, USA) to obtain a Gaussian beam profile and overlaying laser beams. Circular polarized light was obtained by a linear polarizer (LPVISE100-A, Thorlabs) and a quarter-wave plate (AQWP05M- 600, Thorlabs). The laser light was guided into the epi-illuminated confocal microscope (Olympus IX71, Olympus, Japan) by dual-edge beam splitter (z532/633, AHF Analysentechnik AG, Germany) focused by an oil immersion objective (UPLSAPO100XO, NA 1.40, Olympus). The emitted fluorescence was collected through the objective and spatially filtered using a pinhole with 50 μm diameter and spectrally split into donor and acceptor channel by a single-edge dichroic mirror (640DCXR, AHF Analysentechnik AG). Fluorescence emission was filtered (donor: Brightline HC582/75 (AHF Analysentechnik AG) and RazorEdge LP 532 (Laser 2000, Germany); acceptor: Shortpass 750 (AHF Analysentechnik AG) and RazorEdge LP 647 (Laser 2000)) and focused on avalanche photodiodes (SPCM-AQRH-14-TR, Excelitas Technologies, USA). The detector outputs were recorded by a time-correlated single photon counting module (HydraHarp 400, PicoQuant). The setup was controlled by a commercial software package (SymPhoTime64, Picoquant). Data analysis was performed using the "PAM"

software package as described by Schrimpf et al.⁴⁸ Single-molecule events were identified using a two channel APBS-algorithm with a threshold of 10 photons per time window of 500 μ sec and a minimum photon count of 30. Gamma correction was performed using the protocol published by Hellenkamp et al.³⁷ To remove donor or acceptor only events, the ALEX-2CDE filter was applied using an upper threshold of 15.⁴⁹

Fabrication of DNA-Liposome Hybrid Carriers

LUVs were prepared by extrusion of a 2 mM 1-palmitoyl- 2-oleoyl-sn-glycero-3-phosphocholine (POPC, purchased as powder from Sigma-Aldrich and stored dissolved in chloroform) lipid suspension. The lipids were suspended in 1x PBS, sonicated, and extruded through a 200 nm pore size membrane.

The coated liposomes were prepared in aliquots of 100 μ L. 50 μ L of the LUVs were incubated with approximately 1 μ M of the aDBB (pre-annealed with the cholesterol-labelled linker) overnight at room temperature (diluting the POPC lipids to 1.2 mM), rendering VL_{HS}. Subsequently, the triskelion was added to obtain a final concentration of approximately 550 nM and incubated with VL at 4 °C for 50 min (VL_{HS} pre-tempered). This led to a dilution of the linker to approximately 830 nM. Due to the addition of the DNA, the liposomes were effectively diluted by half.

Characterization by Dynamic Light Scattering and ζ -Potential Measurements

Hydrodynamic diameters and ζ -potentials were measured with a ZetaSizer Nano ZSP by Malvern Panalytcs. All samples were measured in disposable cuvettes at a final lipid

concentration of 1 mM in PBS. To measure the ζ -potential, the samples were additionally diluted 1:8 in PBS.

Confocal Microscopy and FRAP Measurements

Confocal microscopy was performed to assess the ability of the DNA structures to coat and deform the membranes of GUVs. Thus, GUVs (including 200:1 (w/w) NBD-labelled PC) were generated by electroformation, using the protocol described in our previous study.³⁴ The linker was annealed with the active hairpin (pre-assembled with the spacer strand as described above) and subsequently added at a concentration of 200 nM and incubated for 2 hours. Finally, the triskelion was added at room temperature and incubated by another hour (2 μ L of 6 μ M T). The spacer strand was purchased with a 5'-ATTO550 modification from IDT. All three arms of the triskelion were labelled with an ATTO647N fluorophore at the 5'-terminal (purchased by IDT). Imaging was conducted using an Olympus F1200 microscope and a 60X oil immersion objective. The samples were illuminated with a 488 nm (NBD-labelled PC lipids to visualize the lipid membranes), 535 nm (ATTO550-labelled spacer), and 635 nm (ATTO647N-labelled triskelion) laser in line-sequential acquisition. The coated GUVs were treated with the displacement strand C for 3 hours to remove the spacer strand and allow the hairpin to close in order to achieve deformation of the vesicles. Before and after this displacement reaction, FRAP analysis was performed to evaluate the diffusion properties of the spacer and triskelion (as an indicator of the extend of DNA polymerization) by bleaching a 3 μ m large area with the 535 nm and 635 nm lasers into the DNA coats. The hyperosmotic pressure was induced by performing the displacement reaction in a solution with an approximately 10% higher osmolarity (by adjusting the glucose concentration).

Calcein Release Experiments

Evidence whether the DNA contraction triggered the release of molecules from the coated liposomes was provided by measuring the leakage of entrapped calcein. POPC lipid films were rehydrated (day 1) in a 60 mM calcein solution diluted in 75 mM Na_2HPO_4 (pH = 7.4). The LUVs were purified from free dye by gel filtration using Sephadex G50. Subsequently, the DNA was added as described in the section above, outlining the DLS experiments. The modified linker in combination with the active hairpin (VL_{HS}) was added at day 1, as well as a version with the inactive hairpin, by omitting S (VL_{H}). On day 2, the T1 triskelion was added to both VL_{HS} and VL_{H} and incubated for 1 hour at 4 °C. Finally, the displacement strand S was added to all samples (to account for dilution effects in the non-trigger-responsive samples), and the fluorescence intensity was recorded over time with a ClarioStar Plus plate reader (BMG Labtech, Germany) excitation wavelength 488 nm \pm 15 nm, emission recorded at 515 nm \pm 20 nm) at room temperature. As a control, C_c was added (altered sequence to prevent hybridization with the spacer strand S). At the end of the acquisition time, 1% of Triton X-100 was added to disrupt the vesicles and record the maximal achievable fluorescence intensity.

Incubation of the DNA-Liposome Hybrid Carriers with HEK293T Cells

The coated liposomes were fabricated to encapsulate doxorubicin (DOX) and incubated with HEK293T cells. DOX is a widely used anti-cancer drug and imposes toxicity towards cells by inducing DNA strand breaks.^{50,51} Coated liposomes were prepared by rehydrating POPC lipids in a solution of 5 mg/mL DOX in sterile 1x PBS. DOX was purchased as powder from Stratech Scientific, UK. The remaining fabrication steps followed the protocol summarized above for calcein. 2500 cells were seeded per well of a 96 well plate and covered by 100 μL DMEM

supplemented with 10% fetal bovine serum and glutamax. The cells were environmentally controlled at 37 °C and 5% CO₂ incubated for three days to allow adherence and confluence. On the third day, the incubation with the coated liposomes was performed. Alongside the VL_{HS}T carriers, the previously established VLT (all prepared with entrapped DOX) was incubated. For each sample, three wells were prepared for incubation by adding 90 µL of sample solution per well for approximately 30 min. Afterwards, 5 µL of the displacement strand D, present in a 30 µM solution in 1x PBS were added. To three separate wells, 95 µL of 1x PBS only was added as a non-toxic control. After an incubation time of approximately 3.5 hours, the supernatant was removed from each well and 30 µL of trypsin solution was added to detach the cells. After 2 min of trypsination, the reaction was blocked by adding 100 µL of fresh culture medium. The cells were then transferred into centrifugation tubes and spun down for 5 min at 300 rcf. Finally, the supernatant was removed and the cell pellets resuspended in 1x PBS and counted using an automated cell counter (Countess, Thermo Scientific, USA) to adjust for deviating cell numbers for the subsequent viability assay. To assess the viability of the HEK293T cells after the treatment, an ATP-sensitive luciferase bioluminescence assay was performed with CellTiter Glo (Promega, USA). To perform the assay, 100 µL of the cells in 1x PBS were pipetted into wells of a black 96-well plate (Greiner, Austria) at an approximate concentration of 10000 per µL. 30 µL of the luciferase buffer were added to each well and incubated for 10 min at 37 °C. The luminescence emission was analyzed using a ClarioStar Plus plate reader.

FIGURES

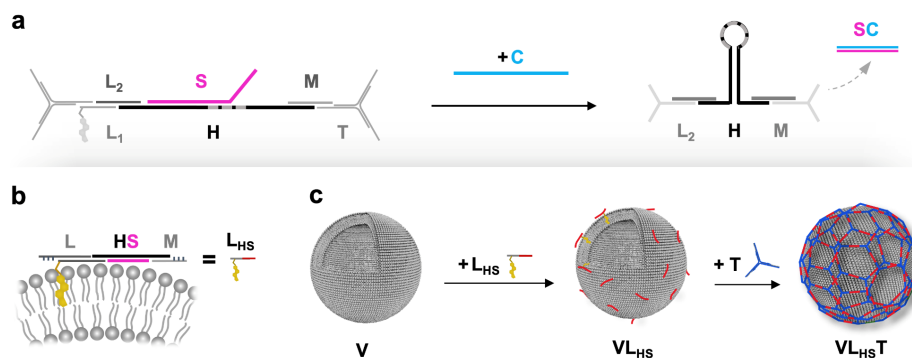


Figure 1. Assembly principle of the active DNA building block and the trigger-responsive DNA-liposomal hybrid nanocarrier. (a) Trigger mechanism of the aDBB. The building block comprises a hairpin H and a pre-annealed, partially complementary sequence S. Mediated by a toehold at the 5'-terminal of S, a complementary trigger strand C hybridizes with S, allowing H to close. This leads to a contraction of the two opposite ends. (b) The aDBB is first annealed with a cholesterol-TEG-modified linker L (comprised of L₂ and the cholesterol-TEG-labelled L₁) and a connecting strand M, to render L_{HS}. (c) L_{HS} is incubated with large unilamellar POPC vesicles (V) and is anchored to the lipid membranes via the cholesterol-TEG modification (rendering VL_{HS}). This allows for polymerization of a triskelion T which is added in the subsequent step on the surface of the vesicles and hybridizes with M and L₁ (resulting in the final structure VL_{HS}T).

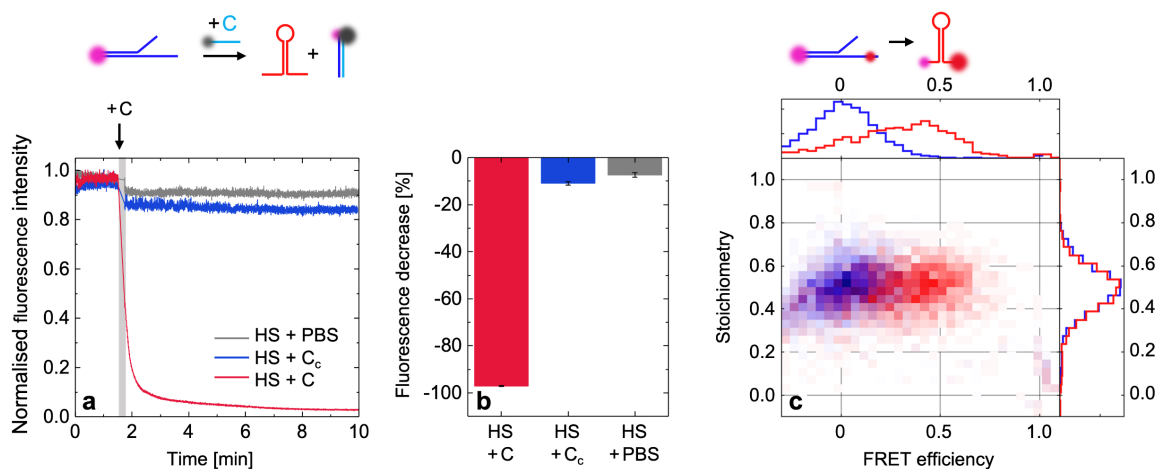


Figure 2. Fluorescence-based assessment of the contraction of the active DNA building block. (a)

The addition of C to the aDBB in solution leads to a steep drop of the fluorescence intensity, indicating high quenching efficiencies of the fluorophore placed at the 3'-terminal of S by the quencher placed at the 5'-terminal of C. (b) The strong relative fluorescence decrease suggests successful displacement of S. A control sequence C_c leads to weak unspecific quenching, comparable to the effect caused by dilution with PBS (error bars represent the standard deviation, n = 3). (c) Single-molecule FRET measurements support the assumption that the displacement of S results in the contraction of the opposite ends of H due to self-hybridization. This is indicated by an increase of the FRET efficiency between a donor-acceptor pair placed at the two opposite ends of H.

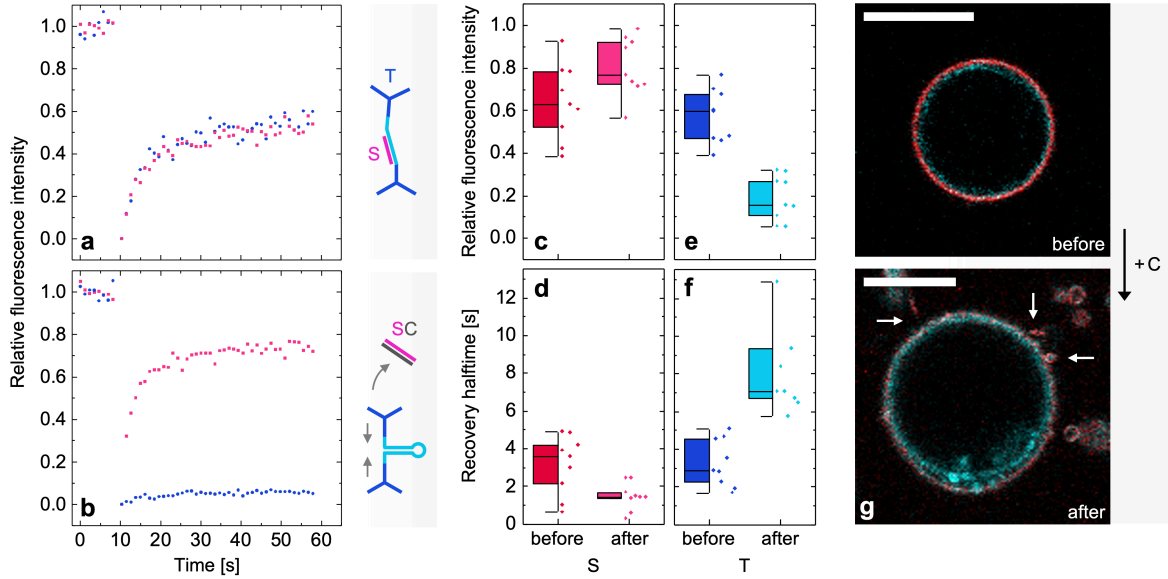


Figure 3. Characterization of DNA-coated GUVs by confocal microscopy and FRAP. (a) Representative FRAP traces recorded on GUVs before the addition of C. S was labelled with ATTO550 (pink data), and T with ATTO647N (blue data). Both species exhibit similar fluorescence recovery dynamics (described by the recovered fluorescence intensities and recovery halftimes obtained from exponential fitting curves, $n = 8$). (b) After the addition of C, the fluorescence recovery kinetics of S and T split into two populations: S is characterized by increased mobility, while T remains mostly static: the recovered relative fluorescence intensity (c) and the recovery halftime (d) of S is slightly higher. By contrast, a drop of the levels of recovered fluorescence (e) and slow recovery kinetics (f) can be observed for T (box plots show the upper and lower quartiles, as well as the mean, $n = 8$). (g) In the presence of a hyperosmotic pressure, visible deformation and tubulation (see arrows) of the coated GUVs could be observed after the displacement of S had been performed (cyan: NBD-labelled PC lipids, red: ATTO647N-labelled T). Scale bars: 10 μm .

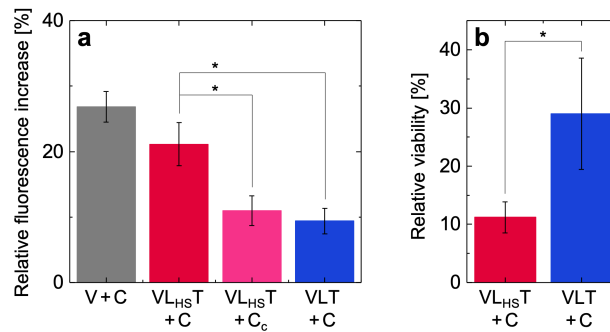


Figure 4. Triggered release of calcein and doxorubicin. (a) The addition of C to VL_{HS}T induces elevated permeability of the carriers to entrapped calcein (VL_{HS}T + C), close to uncoated POPC vesicles (V + C), whereas an inactive version (VLT + C) retains calcein to a larger degree. In comparison to VL_{HS}T + C, the calcein release was significantly lower ($p = 0.0060$, $df = 4$, $t = 5.3227$), similar to the addition of a non-hybridizing C_c to VL_{HS}T ($p = 0.0118$, $df = 4$, $t = 4.3926$). (b) DOX is released from the active carrier upon addition of C (VL_{HS}T + C), provoking cytotoxicity in a HEK293T cell culture. In comparison to VLT, the cytotoxic response is statistically significantly increased ($p = 0.0358$, $df = 4$, $t = 3.1106$). Error bars represent the standard deviation ($n = 3$), the asterisk highlights statistically significant results ($p < 0.05$).

AUTHOR INFORMATION

Corresponding Authors

* Tuomas P. J. Knowles - Yusuf Hamied Department of Chemistry, University of Cambridge, Lensfield Road, Cambridge CB2 1EW, United Kingdom; Email: tpjk2@cam.ac.uk

* Silvia Hernández-Ainsa - Instituto de Nanociencia y Materiales de Aragón, University of Zaragoza-CSIC, Zaragoza 50009, Spain; ARAID Foundation, Government of Aragon, Zaragoza 50018, Spain; Email: silviamh83@unizar.es

Present Addresses

† Department of Biosystems Science and Engineering, ETH Zürich, Mattenstrasse 26, 4058 Basel, Switzerland

‡ Feinberg School of Medicine, Northwestern University, 633 Clark St, Evanston, IL 60208, United States

§ School of Engineering, EPFL, 1015 Lausanne, Switzerland

Author Contributions

The manuscript was written through the contribution of all authors. All authors have given approval to the final version of the manuscript.

ACKNOWLEDGMENT

The research leading to these results has received funding from the European Research Council under the European Union's Seventh Framework Programme (FP7/2007-2013) through the ERC grant PhysProt (Agreement No. 337969). K.N.B., P.S.C., and T.P.J.K. are grateful for financial support from the Biotechnology and Biological Sciences Research Council (BBSRC), the Newman Foundation, the Wellcome Trust and the Cambridge Centre for Misfolding Diseases. D.M. is supported by the Winton Programme for the Physics of Sustainability, as well as the Engineering and Physical Sciences Research Council (EPSRC). T.S. and P.T. gratefully acknowledge funding by the Bavarian Ministry of Science and the Arts through the ONE MUNICH Project "Munich Multiscale Biofabrication" and by the LMU-Cambridge strategic partnership. S.H.A. acknowledges funding by the Gobierno de Aragón-FSE (Research Group E47_20R). The authors would like to thank Prof. Ulrich Keyser, Dr. Florian Buhr, and Anne Jacobs for insightful discussions.

REFERENCES

- (1) Senapati, S.; Mahanta, A. K.; Kumar, S.; Maiti, P. Controlled Drug Delivery Vehicles for Cancer Treatment and Their Performance. *Signal Transduct. Target. Ther.* **2018**, *3* (1), 1–19. <https://doi.org/10.1038/s41392-017-0004-3>.
- (2) Coelho, J. F.; Ferreira, P. C.; Alves, P.; Cordeiro, R.; Fonseca, A. C.; Góis, J. R.; Gil, M. H. Drug Delivery Systems: Advanced Technologies Potentially Applicable in Personalized Treatments. *EPMA J.* **2010**, *1* (1), 164–209. <https://doi.org/10.1007/s13167-010-0001-x>.
- (3) Kumar, V.; Palazzolo, S.; Bayda, S.; Corona, G.; Toffoli, G.; Rizzolio, F. DNA Nanotechnology for Cancer Therapy. *Theranostics* **2016**, *6* (5), 710–725. <https://doi.org/10.7150/thno.14203>.
- (4) Joseph, J.; Baumann, K. N.; Postigo, A.; Bollepalli, L.; Bohndiek, S. E.; Hernández-Ainsa, S. DNA-Based Nanocarriers to Enhance the Optoacoustic Contrast of Tumors In Vivo. *Adv. Healthc. Mater.* **2021**, *10* (2), 2001739. <https://doi.org/10.1002/adhm.202001739>.
- (5) Petschauer, J. S.; Madden, A. J.; Kirschbrown, W. P.; Song, G.; Zamboni, W. C. The Effects of Nanoparticle Drug Loading on the Pharmacokinetics of Anticancer Agents. *Nanomedicine* **2015**, *10* (3), 447–463. <https://doi.org/10.2217/nnm.14.179>.
- (6) De Leo, V.; Milano, F.; Agostiano, A.; Catucci, L. Recent Advancements in Polymer/Liposome Assembly for Drug Delivery: From Surface Modifications to Hybrid Vesicles. *Polymers (Basel)*. **2021**, *13* (7), 1027. <https://doi.org/10.3390/polym13071027>.
- (7) Loomis, K.; McNeeley, K.; Bellamkonda, R. V. Nanoparticles with Targeting, Triggered Release, and Imaging Functionality for Cancer Applications. *Soft Matter* **2011**, *7* (3), 839–

856. <https://doi.org/10.1039/c0sm00534g>.
- (8) Fleige, E.; Quadir, M. A.; Haag, R. Stimuli-Responsive Polymeric Nanocarriers for the Controlled Transport of Active Compounds: Concepts and Applications. *Adv. Drug Deliv. Rev.* **2012**, *64* (9), 866–884. <https://doi.org/10.1016/J.ADDR.2012.01.020>.
- (9) Lee, J. H.; Yeo, Y. Controlled Drug Release from Pharmaceutical Nanocarriers. *Chem. Eng. Sci.* **2015**, *125*, 75–84. <https://doi.org/10.1016/j.ces.2014.08.046>.
- (10) Weber, J.; Beard, P. C.; Bohndiek, S. E. Contrast Agents for Molecular Photoacoustic Imaging. *Nat. Methods* **2016**, *13* (8), 639–650. <https://doi.org/10.1038/nmeth.3929>.
- (11) Fujimoto, J. G.; Schmitt, J.; Swanson, E.; Aguirre, A. D.; Jang, I.-K. The Development of Optical Coherence Tomography. In *Cardiovascular OCT Imaging*; Springer International Publishing, 2020; pp 1–23. https://doi.org/10.1007/978-3-030-25711-8_1.
- (12) Zhao, W.; Zhao, Y.; Wang, Q.; Liu, T.; Sun, J.; Zhang, R. Remote Light-Responsive Nanocarriers for Controlled Drug Delivery: Advances and Perspectives. *Small* **2019**, *15* (45), 1903060. <https://doi.org/10.1002/sml.201903060>.
- (13) Deng, W.; Chen, W.; Clement, S.; Guller, A.; Zhao, Z.; Engel, A.; Goldys, E. M. Controlled Gene and Drug Release from a Liposomal Delivery Platform Triggered by X-Ray Radiation. *Nat. Commun.* **2018**, *9* (1), 1–11. <https://doi.org/10.1038/s41467-018-05118-3>.
- (14) Decuzzi, P.; Cook, A. B. Harnessing Endogenous Stimuli for Responsive Materials in Theranostics. *ACS Nano* **2021**, *15* (2), 2068–2098. <https://doi.org/10.1021/acsnano.0c09115>.

- (15) Chen, L.; Zhang, J.; Lin, Z.; Zhang, Z.; Mao, M.; Wu, J.; Li, Q.; Zhang, Y.; Fan, C. Pharmaceutical Applications of Framework Nucleic Acids. *Acta Pharm. Sin. B* **2021**. <https://doi.org/10.1016/j.apsb.2021.05.022>.
- (16) Douglas, S. M.; Bachelet, I.; Church, G. M. A Logic-Gated Nanorobot for Targeted Transport of Molecular Payloads. *Science* **2012**, 335 (6070), 831–834. <https://doi.org/10.1126/science.1214081>.
- (17) Andersen, E. S.; Dong, M.; Nielsen, M. M.; Jahn, K.; Subramani, R.; Mamdouh, W.; Golas, M. M.; Sander, B.; Stark, H.; Oliveira, C. L. P.; Pedersen, J. S.; Birkedal, V.; Besenbacher, F.; Gothelf, K. V.; Kjems, J. Self-Assembly of a Nanoscale DNA Box with a Controllable Lid. *Nature* **2009**, 459 (7243), 73–76. <https://doi.org/10.1038/nature07971>.
- (18) Madhanagopal, B. R.; Zhang, S.; Demirel, E.; Wady, H.; Chandrasekaran, A. R. DNA Nanocarriers: Programmed to Deliver. *Trends Biochem. Sci.* **2018**, 43 (12), 997–1013. <https://doi.org/10.1016/J.TIBS.2018.09.010>.
- (19) Liphardt, J.; Onoa, B.; Smith, S. B.; Jr, T. I.; Bustamante, C. Reversible Unfolding of Single RNA Molecules by Mechanical Force. *Science* **2001**, 292 (5517), 733–737. <https://doi.org/10.1126/science.1058498>.
- (20) Bercy, M.; Bockelmann, U. Hairpins under Tension: RNA versus DNA. *Nucleic Acids Res.* **2015**, 43 (20), 9928–9936. <https://doi.org/10.1093/nar/gkv860>.
- (21) Strunz, T.; Oroszlan, K.; Schäfer, R.; Güntherodt, H. J. Dynamic Force Spectroscopy of Single DNA Molecules. *Proc. Natl. Acad. Sci. U. S. A.* **1999**, 96 (20), 11277–11282. <https://doi.org/10.1073/pnas.96.20.11277>.

- (22) Gambari, R.; Brognara, E.; Spandidos, D. A.; Fabbri, E. Targeting OncomiRNAs and Mimicking Tumor Suppressor MiRNAs: New Trends in the Development of MiRNA Therapeutic Strategies in Oncology (Review). *Int. J. Oncol.* **2016**, *49* (1), 5–32. <https://doi.org/10.3892/ijo.2016.3503>.
- (23) He, H.; Tian, D.; Guo, J.; Liu, M.; Chen, Z.; Hamdy, F. C.; Helleday, T.; Su, M.; Ying, S. DNA Damage Response in Peritumoral Regions of Oesophageal Cancer Microenvironment. *Carcinogenesis* **2013**, *34* (1), 139–145. <https://doi.org/10.1093/carcin/bgs301>.
- (24) Piwecka, M.; Rolle, K.; Belter, A.; Barciszewska, A. M.; Zywicki, M.; Michalak, M.; Nowak, S.; Naskret-Barciszewska, M. Z.; Barciszewski, J. Comprehensive Analysis of MicroRNA Expression Profile in Malignant Glioma Tissues. *Mol. Oncol.* **2015**, *9* (7), 1324–1340. <https://doi.org/10.1016/j.molonc.2015.03.007>.
- (25) Sanguanini, M.; Baumann, K. N.; Preet, S.; Chia, S.; Habchi, J.; Knowles, T. P. J.; Vendruscolo, M. Complexity in Lipid Membrane Composition Induces Resilience to A β 42 Aggregation. *ACS Chem. Neurosci.* **2020**, *11* (9), 1347–1352. <https://doi.org/10.1021/acscchemneuro.0c00101>.
- (26) Guimarães, D.; Cavaco-Paulo, A.; Nogueira, E. Design of Liposomes as Drug Delivery System for Therapeutic Applications. *Int. J. Pharm.* **2021**, *601*, 120571. <https://doi.org/10.1016/J.IJPHARM.2021.120571>.
- (27) Ohmann, A.; Li, C.-Y.; Maffeo, C.; Al Nahas, K.; Baumann, K. N.; Göpfrich, K.; Yoo, J.; Keyser, U. F.; Aksimentiev, A. A Synthetic Enzyme Built from DNA Flips 107 Lipids per Second in Biological Membranes. *Nat. Commun.* **2018**, *9* (1), 2426.

<https://doi.org/10.1038/s41467-018-04821-5>.

- (28) Burns, J. R.; Göpfrich, K.; Wood, J. W.; Thacker, V. V.; Stulz, E.; Keyser, U. F.; Howorka, S. Lipid-Bilayer-Spanning DNA Nanopores with a Bifunctional Porphyrin Anchor. *Angew. Chemie - Int. Ed.* **2013**, *52* (46), 12069–12072. <https://doi.org/10.1002/anie.201305765>.
- (29) Hernández-Ainsa, S.; Ricci, M.; Hilton, L.; Aviñó, A.; Eritja, R.; Keyser, U. F. Controlling the Reversible Assembly of Liposomes through a Multistimuli Responsive Anchored DNA. *Nano Lett.* **2016**, *16* (7), 4462–4466. <https://doi.org/10.1021/acs.nanolett.6b01618>.
- (30) Göpfrich, K.; Zettl, T.; Meijering, A. E. C.; Hernández-Ainsa, S.; Kocabey, S.; Liedl, T.; Keyser, U. F. DNA-Tile Structures Induce Ionic Currents through Lipid Membranes. *Nano Lett.* **2015**, *15* (5), 3134–3138. <https://doi.org/10.1021/acs.nanolett.5b00189>.
- (31) Czogalla, A.; Franquelim, H. G.; Schwille, P. DNA Nanostructures on Membranes as Tools for Synthetic Biology. *Biophys. J.* **2016**, *110* (8), 1698–1707. <https://doi.org/10.1016/J.BPJ.2016.03.015>.
- (32) Franquelim, H. G.; Khmelinskaia, A.; Sobczak, J.-P.; Dietz, H.; Schwille, P. Membrane Sculpting by Curved DNA Origami Scaffolds. *Nat. Commun.* **2018**, *9* (1), 811. <https://doi.org/10.1038/s41467-018-03198-9>.
- (33) Kocabey, S.; Kempter, S.; List, J.; Xing, Y.; Bae, W.; Schiffels, D.; Shih, W. M.; Simmel, F. C.; Liedl, T. Membrane-Assisted Growth of DNA Origami Nanostructure Arrays. *ACS Nano* **2015**, *9* (4), 3530–3539. <https://doi.org/10.1021/acs.nano.5b00161>.
- (34) Baumann, K. N.; Piantanida, L.; García-Nafría, J.; Sobota, D.; Voitchovsky, K.; Knowles, T. P. J.; Hernández-Ainsa, S. Coating and Stabilization of Liposomes by Clathrin-Inspired

- DNA Self-Assembly. *ACS Nano* **2020**, *14* (2), 2316–2323. <https://doi.org/10.1021/acsnano.9b09453>.
- (35) Ishii, Y.; Yoshida, T.; Funatsu, T.; Wazawa, T.; Yanagida, T. Fluorescence Resonance Energy Transfer between Single Fluorophores Attached to a Coiled-Coil Protein in Aqueous Solution. *Chem. Phys.* **1999**, *247* (1), 163–173. [https://doi.org/10.1016/S0301-0104\(99\)00174-3](https://doi.org/10.1016/S0301-0104(99)00174-3).
- (36) Forster, T. Energiewanderung Und Fluoreszenz. *Naturwissenschaften* **1946**, *33* (6), 166–175. <https://doi.org/10.1007/BF00585226>.
- (37) Hellenkamp, B.; Schmid, S.; Doroshenko, O.; Opanasyuk, O.; Kühnemuth, R.; Rezaei Adariani, S.; Ambrose, B.; Aznauryan, M.; Barth, A.; Birkedal, V.; Bowen, M. E.; Chen, H.; Cordes, T.; Eilert, T.; Fijen, C.; Gebhardt, C.; Götz, M.; Gouridis, G.; Gratton, E.; Ha, T.; Hao, P.; Hanke, C. A.; Hartmann, A.; Hendrix, J.; Hildebrandt, L. L.; Hirschfeld, V.; Hohlbein, J.; Hua, B.; Hübner, C. G.; Kallis, E.; Kapanidis, A. N.; Kim, J.-Y.; Krainer, G.; Lamb, D. C.; Lee, N. K.; Lemke, E. A.; Levesque, B.; Levitus, M.; McCann, J. J.; Naredi-Rainer, N.; Nettels, D.; Ngo, T.; Qiu, R.; Robb, N. C.; Röcker, C.; Sanabria, H.; Schlierf, M.; Schröder, T.; Schuler, B.; Seidel, H.; Streit, L.; Thurn, J.; Tinnefeld, P.; Tyagi, S.; Vandenberk, N.; Vera, A. M.; Weninger, K. R.; Wünsch, B.; Yanez-Orozco, I. S.; Michaelis, J.; Seidel, C. A. M.; Craggs, T. D.; Hugel, T. Precision and Accuracy of Single-Molecule FRET Measurements—a Multi-Laboratory Benchmark Study. *Nat. Methods* **2018**, *15* (9), 669–676. <https://doi.org/10.1038/s41592-018-0085-0>.
- (38) Morzy, D.; Rubio-Sánchez, R.; Joshi, H.; Aksimentiev, A.; Di Michele, L.; Keyser, U. F. Cations Regulate Membrane Attachment and Functionality of DNA Nanostructures. *J. Am.*

- Chem. Soc.* **2021**, *143* (19), 7358–7367. <https://doi.org/10.1021/jacs.1c00166>.
- (39) Zamboni, W. C. Liposomal, Nanoparticle, and Conjugated Formulations of Anticancer Agents. *Clin. Cancer Res.* **2005**, *11* (23), 8230–8234. <https://doi.org/10.1158/1078-0432.CCR-05-1895>.
- (40) Huang, F.; Liao, W. C.; Sohn, Y. S.; Nechushtai, R.; Lu, C. H.; Willner, I. Light-Responsive and PH-Responsive DNA Microcapsules for Controlled Release of Loads. *J. Am. Chem. Soc.* **2016**, *138* (28), 8936–8945. <https://doi.org/10.1021/jacs.6b04773>.
- (41) Sercombe, L.; Veerati, T.; Moheimani, F.; Wu, S. Y.; Sood, A. K.; Hua, S. Advances and Challenges of Liposome Assisted Drug Delivery. *Front. Pharmacol.* **2015**, *6* (DEC), 286. <https://doi.org/10.3389/fphar.2015.00286>.
- (42) Iqbal, N.; Iqbal, N. Human Epidermal Growth Factor Receptor 2 (HER2) in Cancers: Overexpression and Therapeutic Implications. *Mol. Biol. Int.* **2014**, *2014*, 852748. <https://doi.org/10.1155/2014/852748>.
- (43) Sledge, G. W. VEGF-Targeting Therapy for Breast Cancer. *J. Mammary Gland Biol. Neoplasia* **2005**, *10* (4), 319–323. <https://doi.org/10.1007/s10911-006-9005-5>.
- (44) Bunker, A.; Magarkar, A.; Viitala, T. Rational Design of Liposomal Drug Delivery Systems, a Review: Combined Experimental and Computational Studies of Lipid Membranes, Liposomes and Their PEGylation. *Biochim. Biophys. Acta - Biomembr.* **2016**, *1858* (10), 2334–2352. <https://doi.org/10.1016/j.bbamem.2016.02.025>.
- (45) Dore-Savard, L.; Lee, E.; Kakkad, S.; Popel, A. S.; Bhujwala, Z. M. The Angiogenic Secretome in VEGF Overexpressing Breast Cancer Xenografts. *Sci. Rep.* **2016**, *6* (1), 1–10.

<https://doi.org/10.1038/srep39460>.

- (46) Mi, P. Stimuli-Responsive Nanocarriers for Drug Delivery, Tumor Imaging, Therapy and Theranostics. *Theranostics* **2020**, *10* (10), 4557–4588. <https://doi.org/10.7150/THNO.38069>.
- (47) Müller, B. K.; Zaychikov, E.; Bräuchle, C.; Lamb, D. C. Pulsed Interleaved Excitation. *Biophys. J.* **2005**, *89* (5), 3508–3522. <https://doi.org/10.1529/biophysj.105.064766>.
- (48) Schrimpf, W.; Barth, A.; Hendrix, J.; Lamb, D. C. PAM: A Framework for Integrated Analysis of Imaging, Single-Molecule, and Ensemble Fluorescence Data. *Biophys. J.* **2018**, *114* (7), 1518–1528. <https://doi.org/10.1016/j.bpj.2018.02.035>.
- (49) Tomov, T. E.; Tsukanov, R.; Masoud, R.; Liber, M.; Plavner, N.; Nir, E. Disentangling Subpopulations in Single-Molecule FRET and ALEX Experiments with Photon Distribution Analysis. *Biophys. J.* **2012**, *102* (5), 1163–1173. <https://doi.org/10.1016/j.bpj.2011.11.4025>.
- (50) Lopes De Menezes, D. E.; Kirchmeier, M. J.; Gagne, J. F.; Pilarski, L. M.; Allen, T. M. Cellular Trafficking and Cytotoxicity of Anti-CD19-Targeted Liposomal Doxorubicin in B Lymphoma Cells. *J. Liposome Res.* **1999**, *9* (2), 199–228. <https://doi.org/10.3109/08982109909024786>.
- (51) Chatterjee, K.; Zhang, J.; Honbo, N.; Karliner, J. S. Doxorubicin Cardiomyopathy. *Cardiology* **2010**, *115* (2), 155–162. <https://doi.org/10.1159/000265166>.